

A 51-dB signal-to-noise ratio carrier-envelope offset frequency in an environmentally stabilized polarization-maintaining optical frequency comb

Yuyao Zong(宗玉瑶), Yi Han(韩羿), Jiawei Liu(刘佳伟), Cheng Ci(慈骋), Zhenyu Xue(薛振宇), and Shiying Cao(曹士英)

Citation: Chin. Phys. B, 2026, 35 (**6**): 064206. DOI: 10.1088/1674-1056/ae0924
http://cpb.iphy.ac.cn; http://iopscience.iop.org/cpb

What follows is a list of articles you may be interested in

Frequency-modulated continuous-wave multiplexed gas sensing based on optical frequency comb calibration

Linhua Jia(贾琳华), Xinghua Qu(曲兴华), and Fumin Zhang (张福民)
Chin. Phys. B, 2024, 33 (**9**): 094201. DOI: 10.1088/1674-1056/ad5980

Numerical study of converting beat-note signals of dual-frequency lasers to optical frequency combs by optical injection locking of semiconductor lasers

Chenhao Liu(刘晨浩), Haoshu Jin(靳昊澍), Hui Liu(刘辉), and Jintao Bai(白晋涛)
Chin. Phys. B, 2022, 31 (**8**): 084205. DOI: 10.1088/1674-1056/ac649a

Precise determination of characteristic laser frequencies by an Er-doped fiber optical frequency comb

Shiying Cao(曹士英), Yi Han(韩羿), Yongjin Ding(丁永今), Baike Lin(林百科), and Zhanjun Fang(方占军)
Chin. Phys. B, 2022, 31 (**7**): 074207. DOI: 10.1088/1674-1056/ac5608

Generation of stable and tunable optical frequency linked to a radio frequency by use of a high finesse cavity and its application in absorption spectroscopy

Yueting Zhou(周月婷), Gang Zhao(赵刚), Jianxin Liu(刘建鑫), Xiaojuan Yan(闫晓娟), Zhixin Li(李志新), Weiguang Ma(马维光), and Suotang Jia(贾锁堂)
Chin. Phys. B, 2022, 31 (**6**): 064206. DOI: 10.1088/1674-1056/ac4905

All polarization-maintaining Er:fiber-based optical frequency comb for frequency comparison of optical clocks

Pan Zhang(张攀), Yan-Yan Zhang(张颜艳), Ming-Kun Li(李铭坤), Bing-Jie Rao(饶冰洁), Lu-Lu Yan(闫露露), Fa-Xi Chen(陈法喜), Xiao-Fei Zhang(张晓斐), Qun-Feng Chen(陈群峰), Hai-Feng Jiang(姜海峰)[‡], and Shou-Gang Zhang(张首刚)
Chin. Phys. B, 2022, 31 (**5**): 054210. DOI: 10.1088/1674-1056/ac40f6

A 51-dB signal-to-noise ratio carrier-envelope offset frequency in an environmentally stabilized polarization-maintaining optical frequency comb

Yuyao Zong(宗玉瑶)[1,2,3,†], Yi Han(韩羿)[2,3,†], Jiawei Liu(刘佳伟)[2,3], Cheng Ci(慈骋)[1], Zhenyu Xue(薛振宇)[1], and Shiying Cao(曹士英)[2,3,‡]

[1] *College of Information Engineering, China Jiliang University, Hangzhou* 310018, *China*
[2] *Division of Time and Frequency Metrology, National Institute of Metrology, Beijing* 100029, *China*
[3] *Key Laboratory of State Administration for Market Regulation, Time Frequency and Gravity Primary Standard, Beijing* 100029, *China*

(Received 9 August 2025; revised manuscript received 8 September 2025; accepted manuscript online 19 September 2025)

A femtosecond optical frequency comb (OFC) based on a laser with a nonlinear amplification loop mirror mode-locking mechanism is proposed. The laser adopts a fully polarization-maintaining (PM) structure, which can realize self-starting mode-locking at the center wavelength of 1560.2 nm with a 195.65 MHz repetition rate at a pump power of 630 mW, and the frequency stability after phase-locking is 1.95×10^{-12} with a 1-s averaging time. Through a homemade f–$2f$ interferometer, the detected free-running $f_{\rm ceo}$ signal exhibits a signal-to-noise ratio (SNR) as high as 51 dB. After phase-locking, $f_{\rm ceo}$ has a frequency stability of 1.17×10^{-11} with a 1-s averaging time.

Keywords: optical frequency comb, Er-doped mode-locked laser, $f_{\rm ceo}$ linewidth optimization, pre-chirp amplification

PACS: 42.55.Wd, 42.65.–k, 06.30.Ft

DOI: 10.1088/1674-1056/ae0924 **CSTR:** 32038.14.CPB.ae0924

1. Introduction

Optical frequency combs (OFCs) are of broad interest due to their long-standing role as a bridge between optical and radio frequencies. In the past decade, low-noise OFCs have been widely used in the fields of precision instrument measurement,[1,2] absolute frequency calibration,[3,4] optical clock comparison,[5–7] and molecular spectroscopy.[8–11] In recent years, the progressively enhanced stability of atomic clocks has driven continuous improvements in the performance specifications of OFCs, which serve as indispensable tools for optical atomic transition comparisons.[12,13] Early OFCs primarily employed solid-state lasers as their light sources.[14] Progress in nonlinear optics and optical communication technologies facilitates the implementation of cost-effective laser devices, such as fiber lasers and semiconductor lasers, thereby enhancing system affordability and practical performance.[15] The OFC based on a passive mode-locked Er-doped fiber laser has garnered substantial research interest due to its exceptional environmental stability and superior system integration capabilities.[16–18]

The noise of the laser is one of the decisive factors determining the linewidth of $f_{\rm ceo}$. In turn, laser noise is influenced by different passive mode-locking mechanisms. Material saturable absorbers (SAs) exhibit a long relaxation time, which introduces additional inter-pulse phase jitter.[19] Moreover, even when fully saturated, SAs still exhibit certain residual loss, ultimately leading to higher laser noise.[20] The NPR structure, which relies on nonlinear polarization rotation, makes it difficult to achieve a fully polarization-maintaining (PM) architecture. This inherent limitation makes the system more vulnerable to environmental perturbations, resulting in elevated low-frequency phase noise.[21] Fortunately, PM–NALM-based lasers have found extensive applications in optical frequency comb research owing to their high stability and integration capability.[22,23] Furthermore, pulse chirp and intracavity dispersion play a vital role in reducing timing jitter,[19] which consequently affects the linewidth of $f_{\rm ceo}$. Additionally, the $f_{\rm ceo}$ is also related to the pump source, as fluctuations in its output intensity induce variations in the gain of the intracavity gain fiber. These variations subsequently perturb nonlinear processes within the cavity and are converted into phase noise.[24,25]

In this paper, we demonstrate an all-PM fiber-based frequency comb utilizing an erbium-doped fiber laser with NALM mode-locking technology. Experimental results reveal that the laser achieves self-starting mode-locking in the stretched-pulse regime at a pump power threshold of 630 mW. The repetition rate is up to 195.65 MHz, which is controlled by an intracavity piezoelectric transducer (PZT). The short-term stability is 1.95×10^{-12} with an averaging time of 1 s. The $f_{\rm ceo}$

[†]These authors contributed to this work equally.
[‡]Corresponding author. E-mail: caoshiying@nim.ac.cn

© 2026 Chinese Physical Society and IOP Publishing Ltd. All rights, including for text and data mining, AI training, and similar technologies, are reserved.

signal with an SNR of up to 51 dB is obtained by expanding the spectrum, frequency doubling, and phase-locking of the laser. This makes the f_{ceo} signal more suitable for long-term locking requirements. The short-term stability after phase-locking is 1.17×10^{-11} with an averaging time of 1 s.

2. Experimental setup

2.1. Laser setup

The schematic diagram of the figure-9 laser is shown in Fig. 1. Fast-axis blocked PM devices are employed to enhance environmental stability. The group velocity dispersion (GVD) of the PM passive fiber (PM1550) is about -22 fs^2/mm. A 41-cm-long, highly Er-doped fiber (EDF1, Liekki Er80-4/125-PM) with a core absorption peak of 80 dB/m at 1530 nm not only serves as the gain medium but also provides nominal dispersion (GVD = 20 fs^2/mm). The gain fiber is spliced between a 980/1550-nm wavelength division multiplexer (WDM1) and a collimator (Col1). A 980-nm laser diode (Pump1, II–VI CM97-990-76) together with a current controller (Thorlabs LDC8020) serves as the pump. The pigtail length of Col1 is cut as short as possible, while the pigtails of Col2 and the WDM remain longer. This operation places EDF1 asymmetrically, resulting in a nonlinear phase difference between the counter-propagating beams. To minimize the relative intensity noise, timing jitter, and f_{ceo} noise, we managed the intracavity net dispersion close to zero by adjusting the passive fiber length.[19] The parameters of every segment of fiber in the fiber loop are illustrated in Table 1, and the net dispersion is calculated to be -1150 fs^2.

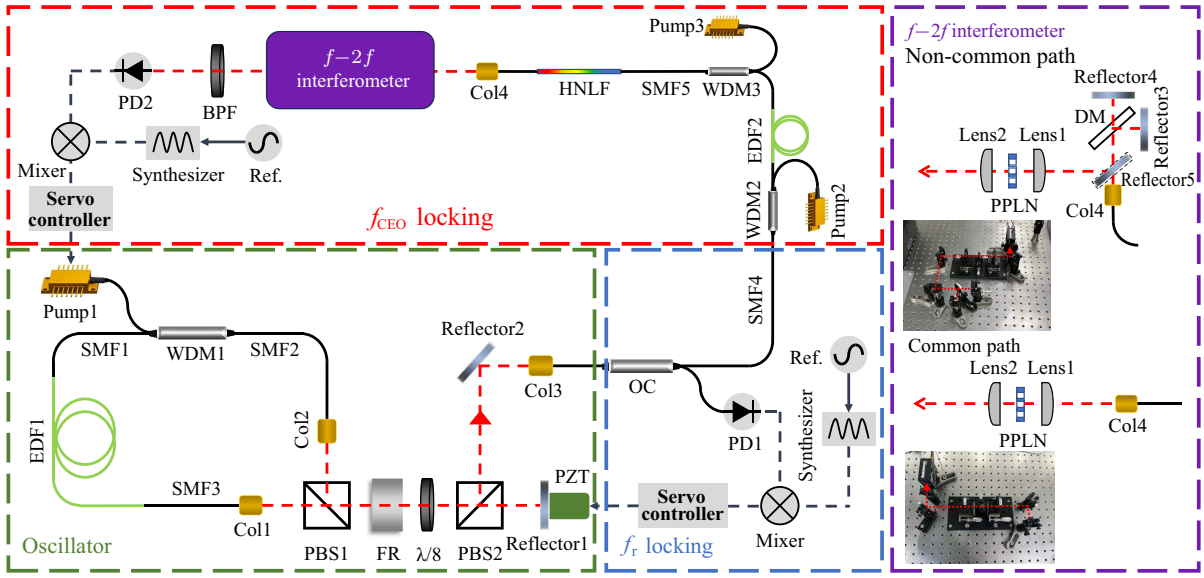


Fig. 1. Schematic diagram of PM optical frequency comb. SMF: polarization maintaining 1550 panda fiber; EDF: polarization maintaining erbium-doped fiber; Col: collimator; PBS: polarization beam splitter; FR: 45° faraday rotator; $\lambda/8$: 1/8 waveplate; PZT: piezo-electric transducer; WDM: wavelength division multiplexing; OC: 50:50 optical coupler; PD: photo detector; Ref.: reference frequency; HNLF: high nonlinear fiber; PPLN: periodically poled lithium niobate; BPF: band-pass filter; DM: dichroic Mirror.

Table 1. The GVD and length of fibers in the all-PM NALM.

	SMF1	SMF2	SMF3	EDF1	Total dispersion (fs^2)
GVD (fs^2/mm)	–22	–22	–22	20	–1150
Length (mm)	125	260	40	410	

We manually rotated Col2 until the reflected ASE power from PBS1 reached its maximum, which ensures that the linearly polarized light is incident on PBS1 as s-state polarized light with low loss. For aligning Col1, continuous-wave laser output must first be achieved; when the p-state polarized light from PBS1 is coupled into Col1 at an angle parallel to the slow axis of the fiber, the output power of PBS2 is maximized. This method of improving spatial light calibration makes the laser structure more compact compared with additional half-waveplates.[26] The combined beams from PBS1 pass through a non-reciprocal phase shifter composed of a Faraday rotator (FR) and a 1/8-wave plate ($\lambda/8$). Then, two orthogonal beams that accumulate nonlinear phase difference in the fiber loop project onto the p and s directions of PBS2 and interfere with each other. By rotating $\lambda/8$, the transmission curve of the cavity can be adjusted. When the angle between the fast axis of the waveplate and the x-axis is 45°, passing through the $\lambda/8$ twice will accumulate a phase shift of $\pi/2$; the configuration can work as an artificial saturable or a reverse SA.[27] An appropriate angle can cause only the high-power pulses to pass through PBS2, significantly reducing the mode-locking threshold. A silver mirror is placed at the end of the free-space section to reflect the pulses back to the loop. The geometrical length of the free-space section in one round trip is approximately 120 mm, which matches the working distance of the collimators.

2.2. PM OFC setup

Output pulses from PBS2 are coupled into a 50:50 PM optical coupler (OC) through Col3 and divided into two channels, one for detecting f_r and the other for further amplification and compression to obtain high-energy ultrashort pulses. The f_r signal is detected by a 2 GHz photodetector (EOT ET-3000A). The fiber length between Col3 and OC is $\sim$ 13 cm. The amplifier consists of two 980 nm laser diodes (Pump2 and Pump3, II–VI CM97-990-76) and two PM WDMs that bidirectionally pump a 135 cm long PM EDF (EDF2, Liekki Er80-4/125-PM). The common ports of the WDMs are fixed at 10 cm. We introduce an appropriate pre-chirp for the pulses by controlling the length of the PM1550 fiber (SMF-4) between WDM2 and the OC, which in turn affects the self-phase modulation (SPM) effect of the pulse propagation in EDF2. In the pigtail of the output section of the amplifier (SMF-5), the amplified higher-order soliton exhibits a periodic evolution due to the interaction between the GVD and SPM. Therefore, by controlling the length of SMF-5, we make the pulse width reach its narrowest and fiber-couple it to a 45 cm PM high nonlinear fiber (HNLF , OFS HNLF–PM, GVD $= -6.37$ fs^2/mm@1550 nm) to obtain a supercontinuum spectrum that covers one octave. Finally, the one-octave spectrum is space-coupled to an f–$2f$ interferometer through Col4 for detecting and stabilizing f_{ceo}. The long wavelength part is frequency doubled using a periodically poled lithium niobate crystal (PPLN) with a light transmission distance of 8 mm. The combined 2nd harmonic and the fundamental radiation at the center wavelength around 1000 nm are filtered out by a band-pass filter and interfered with a high-sensitivity fast PIN photodetector (PD2, Menlo-systems FPD 310-F). In the experiment, a non-common path interferometer was first constructed to investigate the maximum achievable SNR of f_{ceo} through precise time-delay adjustment. Subsequently, to mitigate mechanical vibration-induced environmental noise, the length of the Col4 pigtail fiber was carefully optimized to maximize the f_{ceo} SNR.

The f_r and f_{ceo} stabilization circuit portions comprise low-noise amplifiers, mixers, and band-pass filters. A 10-MHz hydrogen maser (H-maser) signal, periodically calibrated by a caesium (Cs) atomic fountain clock,[28,29] along with a frequency synthesizer (R & S SMA 100A) locked to this signal, was used to generate the reference signals for f_{ceo} and f_r, respectively. The generated f_r error signal was fed back to the PZT through a high-speed servo, and the f_{ceo} error signal was fed back to the oscillator pump current via another servo.

3. Results and discussion

3.1. Mode-locked characteristics

The laser initiates continuous-wave (CW) oscillation at a threshold pump power of 50 mW. When the pump power is increased to 630 mW, self-starting mode-locking is achieved in the single-pulse regime without any CW components at the central wavelength. The mode-locked state remains stable until the pump power is reduced to 300 mW, demonstrating a wide operating range of 330 mW for robust mode-locking maintenance.

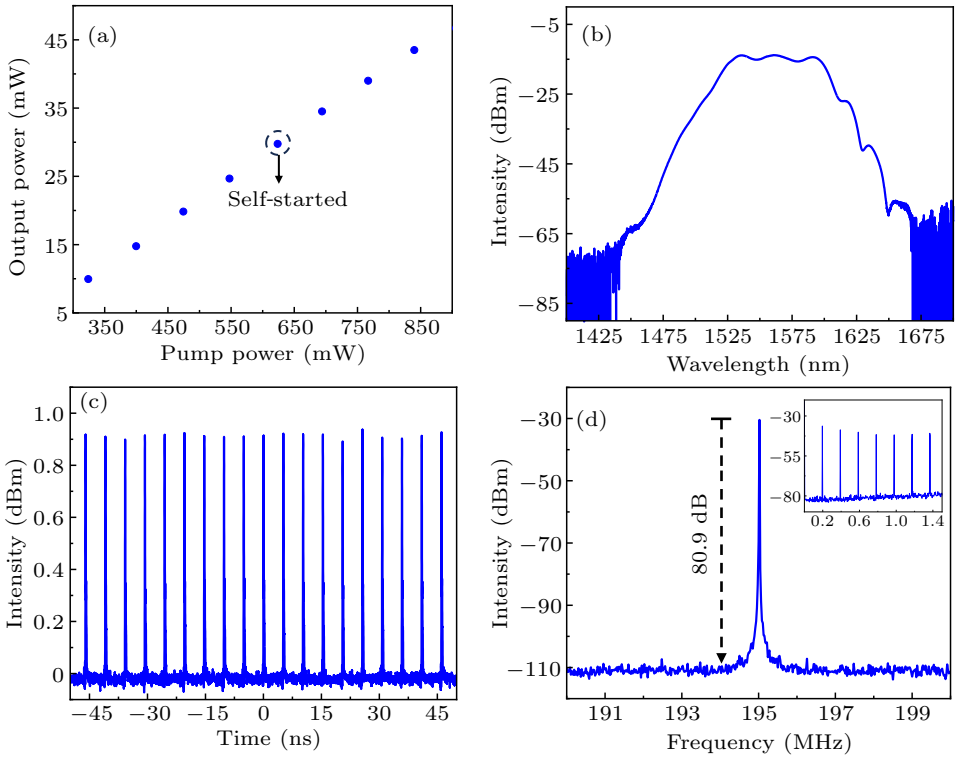


Fig. 2. (a) Variation of the output power with the pump power. (b) Self-started optical spectrum at the pump power of 630 mW. (c) Measured oscilloscope trace of the single pulse trains at the pump power of 630 mW. (d) Measured RF spectrum of the fundamental repetition frequency. Inset: the 1.5-GHz bandwidth RF spectrum.

The mode-locked pulses from PBS2 are spatially coupled into the fiber via Col3, achieving a coupling efficiency of $\sim 75\%$. As depicted in Fig. 2(a), the average mode-locked power measured after Col3 exhibits a linear dependence on the pump power. Figure 2(b) illustrates the self-started spectrum at the pump power of 630 mW. The full width at half maximum (FWHM) of the spectrum measured at a resolution of 0.5 nm is 67.9 nm with a central wavelength of 1560.2 nm. The time–domain single-pulse trains recorded by an 8-GHz-bandwidth oscilloscope (Keysight DSOV08A) is shown in Fig. 2(c). The pulse period is around 5.11 ns. Figure 2(d) shows the radio frequency (RF) spectrum measured by an RF spectrum signal analyzer (Agilent N9340B). The fundamental repetition rate frequency is located at 195.65 MHz with a resolution bandwidth (RBW) of 300 Hz and a span of 10 MHz (190.4 MHz to 200.4 MHz), consistent with the temporal pulse period shown in Fig. 2(c). The SNR reaches 80.9 dB, demonstrating exceptional pulse-to-pulse stability. Inset in Fig. 2(d) shows the RF spectrum with a 1.5-GHz span and a resolution bandwidth of 300 kHz. The harmonic signals exhibit monotonically decreasing intensity from low to high frequencies without periodic modulation, confirming stable single-pulse mode-locked operation.

3.2. Establishment of the OFC

The seed pulses have an average power of approximately 13 mW after being split by the OC. With both Pump2 and Pump3 set to 900 mW, the amplified pulses achieve an average power of 405 mW and a pulse energy of 2.07 nJ. Figure 3(a) summarizes the optical spectra relative to the length of SMF-4 after amplification. When the fiber is 195.5 cm, the FWHM of the spectrum measured at a resolution of 0.5 nm is 81 nm. Further decrease in the fiber length to 88 cm leads to a broader FWHM of 111 nm, corresponding to a transform-limited pulse width of about 33 fs (Gaussian fitting). Then, the amplified pulses are compressed in the pigtail of WDM3. The pulse width is characterized using a commercial autocorrelator (APE Pulsecheck 150). Figure 3(b) systematically illustrates the evolution of autocorrelation traces *versus* SMF-5 length. Although the pulse width reaches 77 fs at a fiber length of 161.5 cm, higher-order soliton fission leads to the emergence of subsidiary pulses alongside the main pulse peak. As the fiber length decreases, the subsidiary pulses gradually converge toward the main peak, eventually evolving into low-intensity residual wing structures. At a fiber length of 54 cm, the pulse quality improves significantly with a measured pulse width of 82 fs. Subsequently, the compressed pulses are coupled into the PM–HNLF, generating an octave-spanning supercontinuum spectrum as illustrated in Fig. 3(c). The generated supercontinuum exhibits a starting wavelength below 1000 nm and extends beyond 2000 nm. The spectrum covering one octave is coupled into an f–$2f$ interferometer to generate f_{ceo} signal. A fan-out PPLN crystal with an optical path length of 8 mm can double the frequency components in the 2000-nm to 2200-nm range of the spectrum to 1000-nm to 1100-nm. We continuously adjust the PPLN period and record the corresponding frequency doubling, as shown in Fig. 3(d). Note that the fundamental and frequency-doubled light can reach the highest intensity at 1000 nm.

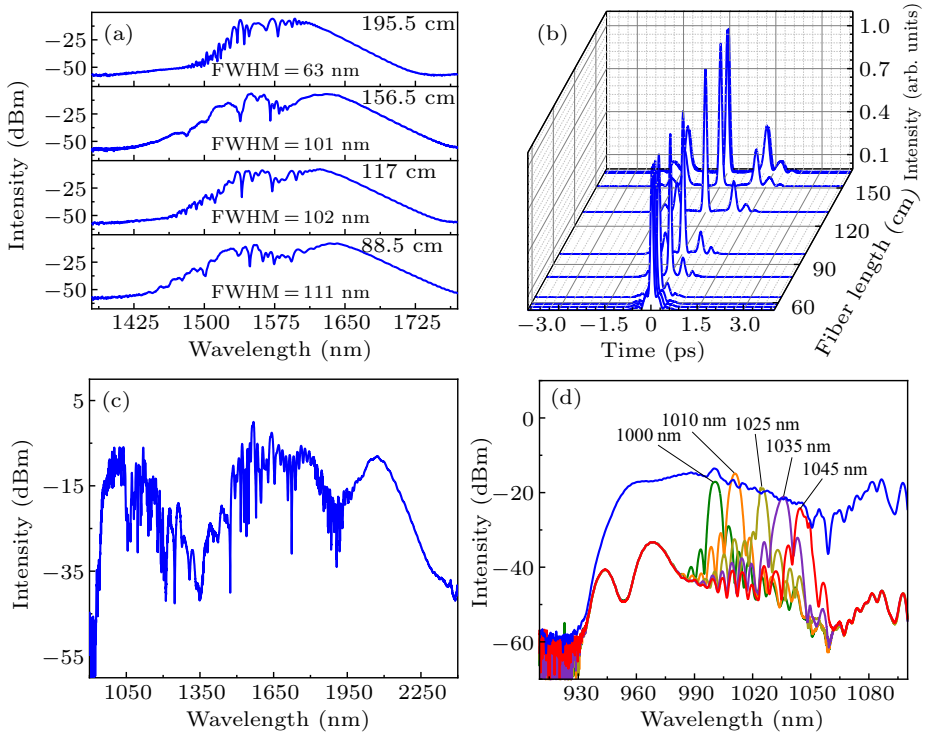


Fig. 3. (a) The amplified spectrum relative to the length of the fiber. (b) Evolution of autocorrelation traces with fiber length. (c) Octave-spanning supercontinuum spectrum after PM–HNLF. (d) Comparisons between the fundamental wave and PPLN-generated second-harmonic.

For f_{ceo} detection, both the frequency-doubled light and the fundamental light are combined and co-coupled into PD2. As determined from Fig. 3(d), the operating wavelengths are optimized to 1000 nm for the two optical components. To avoid detector saturation, a narrowband optical filter with a bandwidth of ±5 nm is installed before the detector to selectively transmit only the 1000 ± 5-nm radiation while rejecting other wavelengths.

3.3. Optimization of f_{ceo} SNR

The f_{ceo} signal was successfully detected via the non-common path configuration, as shown in Fig. 4(a) (250 MHz span, 100 kHz RBW). The SNR of f_{ceo} was optimized through adjustment of the delay arm. Figure 4(b) illustrates the relationship between translation stage displacement and f_{ceo} SNR. The experimental results reveal that the f_{ceo} signal appears and disappears within an extremely narrow displacement range of around 2 mm, demonstrating remarkable constraints in the adjustable range. Benefiting from the highly robust environmental disturbance resistance of the all-PM structure and the low-loss free-space optical design, the SNR can exceed 50 dB under fine tuning.

To optimize the f_{ceo} signal performance, we also conducted a comparative analysis of two current controllers (Thorlabs LDC8020 and CLD1015) with distinct current noise characteristics to systematically investigate the transfer of laser noise to f_{ceo} signal degradation. The key specifications of both controllers are summarized in Table 2, revealing that the LDC8020 produces twice the current noise of the CLD1015. Figures 4(c) and 4(d) respectively present the f_{ceo} signals obtained under identical pump power using the LDC8020 current controller and CLD1015 current controller. Lorentzian fitting in linear coordinates (300-Hz RBW) demonstrates that reducing the controller noise can significantly compress the f_{ceo} linewidth, with the narrowest linewidth of 10.4 kHz achieved in our experiment. The insets show the f_{ceo} RF spectra in logarithmic coordinates (40-MHz span, 100-kHz RBW), where the SNR reaches 51.1 dB after switching to the low-noise controller. This narrow f_{ceo} linewidth is more conducive to achieving long-term robust locking. To better suppress in-loop noise, we replaced the interferometer with a common-path structure as shown in Fig. 1, and adjusted the time delay between long-wavelength and short-wavelength pulse components by optimizing the length of the Col4 pigtail fiber (PM1550). The relationship between the fiber length and f_{ceo} SNR variation is illustrated in Fig. 4(e). When the fiber length is 143 mm, the SNR reaches 48 dB (40-MHz span, 100-kHz RBW), as shown in Fig. 4(f). Such a high SNR is sufficient to ensure long-term f_{ceo} locking.

Table 2. Parameters of the current controllers.

	Thorlabs LDC8020	Thorlabs CLD1015
Current (mA)	∼ 2000	∼ 1500
Noise RMS (μA)	20	10
3-dB-bandwidth (kHz)	DC ∼ 30	DC ∼ 250

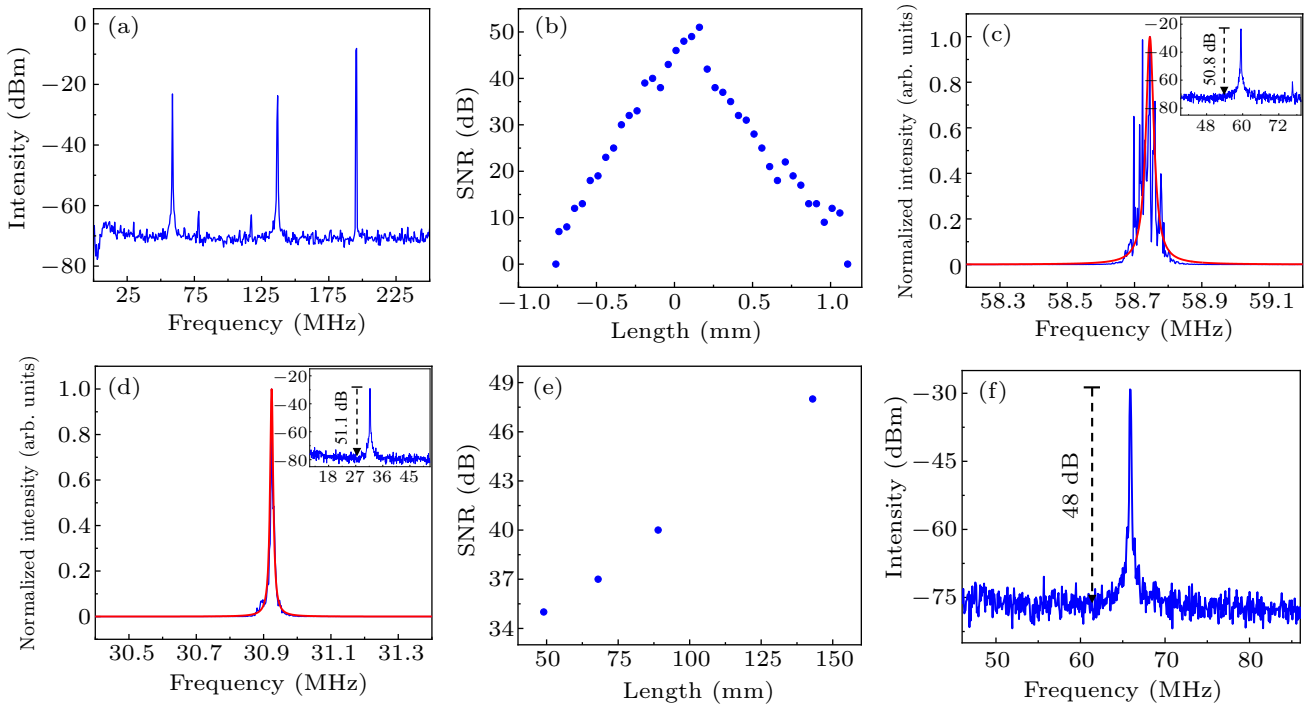


Fig. 4. (a) In-loop RF spectrum of free-running f_{ceo} (100-kHz RBW). (b) Variation of f_{ceo} SNR with the displacement length of delay arm in the non-common path configuration. (c)–(d) Free-running f_{ceo} RF spectra with Lorentzian fitting in linear coordinates (300-Hz RBW), driven by LDC8020 and CLD1015 current controllers, respectively. Inset: f_{ceo} signal in logarithmic coordinates (100-kHz RBW). (e) The f_{ceo} SNR as a function of the Col4 pigtail length in a common-path configuration. (f) Free-running f_{ceo} RF spectrum in the common-path configuration. (100-kHz RBW).

A phase noise analyzer (Agilent Technologies E5052B) was used to study the noise characteristics of the OFC. Figure 5(a) shows the single-side phase noise PSDs of the mode-locked laser operating with a Thorlabs LDC8020 (blue solid line) and a Thorlabs CLD1015 (green solid line) current source in a free-running state. The timing jitters of the repetition rate utilizing two current sources under free-running state are calculated to be 571 fs and 518 fs (integrated from 100 Hz to 1 MHz), respectively. It can be seen that when using the Thorlabs CLD1015 current source with lower current noise, the laser exhibits lower phase noise. The red solid line represents the state of the laser under PZT locking with the Thorlabs CLD1015 current source. The comparison reveals that the phase-locked loop can significantly reduce phase noise in the low-frequency range of 1 Hz to 30 Hz; the calculated time jitter is 601 fs (integrated from 100 Hz to 1 MHz). Figure 5(b) shows the phase noise PSDs of the locked f_{ceo}. The inset of Fig. 5(b) is the phase-locked f_{ceo} signal with a 1-MHz span centered at 20 MHz. The characteristic servo bump at 150 kHz is consistent with the phase noise PSD. Figures 5(c) and 5(d) present the Allan deviations of the phase-locked f_{r} and f_{ceo} signals, respectively. Insets are the frequency deviations of individual signals after stabilization. The in-loop frequency stabilities (1-s average time) reach 1.95×10^{-12} for f_{r} and 1.17×10^{-11} for f_{ceo}, and the calculated standard deviations are 0.379 mHz for the f_{r} signal and 0.234 mHz for the f_{ceo} signal, respectively. Furthermore, the frequency stability can be further improved by subsequently locking the high-order harmonics of the repetition rate to a microwave reference[26] or by locking the comb teeth to an optical reference.[30]

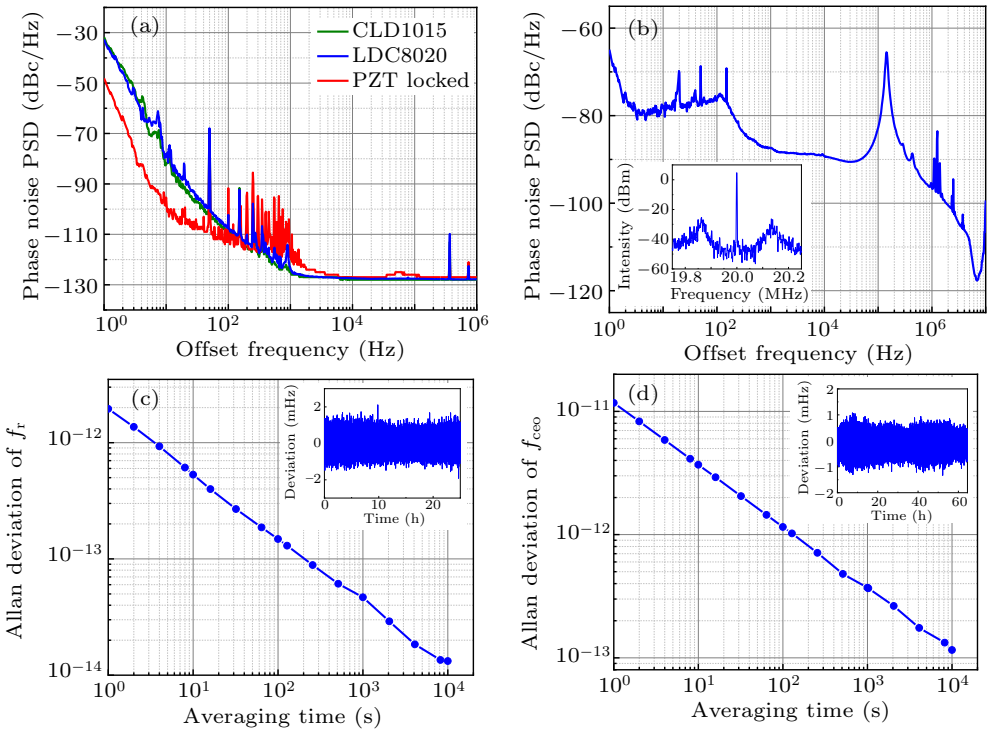


Fig. 5. (a) The single-side phase noise PSDs. Free-running operation powered by Thorlabs LDC8020 (blue solid line). Free-running operation powered by Thorlabs CLD1015 (green solid line). PZT-locked state powered by CLD1015 (red solid line) (b) single-side phase noise PSDs of the locked f_{ceo}. Inset: in-loop RF spectrum of f_{ceo} signal with 3-kHz RBW. Panels (c) and (d) are in-loop frequency stabilities of stabilized f_{r} and f_{ceo} signals. Insets: the frequency deviation of the stabilized signal.

4. Conclusion and perspectives

We propose a fiber femtosecond OFC based on a NALM mode-locked laser. The laser adopts a fully PM structure, and mode-locking in the stretched-pulse regime is realized at a center wavelength of 1560.2 nm. The repetition rate is 195.65 MHz. The short-term stability reaches 1.95×10^{-12} with a 1-s averaging time under phase-locked operation. We implemented a non-common-path f–$2f$ interferometer, where precise adjustment of the delay arm enabled optimization of the f_{ceo} SNR up to 51 dB (100 kHz RBW). Our investigation of laser noise impact on the f_{ceo} revealed that under identical pump currents, the Thorlabs CLD1015 current source demonstrated superior noise performance compared to the Thorlabs LDC8020. While the effect on f_{ceo} SNR was minimal, we observed a significant reduction in the f_{ceo} linewidth from 28.3 kHz to 10.4 kHz (Lorentz fit) when using the Thorlabs CLD1015. The phase-locked signal achieves a short-term stability of 1.17×10^{-11} with a 1-s averaging time, and the calculated timing jitter is 601 fs. This high-SNR f_{ceo} and environmentally robust OFC will be beneficial for long-term frequency measurement of optical frequencies and long-term frequency comparison of different optical clocks.

Acknowledgements

Project supported by the National Key Research and Development Program of China (Grant No. 2021YFF0603801), and the Scientific Research Foundation of the National Institute of Metrology, China (Grant Nos. AKYZD2411 and AKYZD2511).

References

[1] Fortier T and Baumann E 2019 *Commun. Phys.* **2** 153
[2] Holzwarth R, Udem T, Hänsch T W, Knight J C, Wadsworth W J and Russell P S J 2000 *Phys. Rev. Lett.* **85** 2264
[3] Stone J A and Patrick E 2010 *J. Res. Natl. Inst. Stand. Technol.* **115** 413
[4] Chang L, Liu S and Bowers J E 2022 *Nat. Photonics* **16** 95
[5] Diddams S A 2010 *J. Opt. Soc. Am. B* **27** B51
[6] Zhang P, Zhang Y, Li M, Rao B, Yan L, Chen F, Zhang X, Chen Q, Jiang H and Zhang S 2022 *Chin. Phys. B* **31** 054210
[7] Kim E B, Park C Y, Yu D H, Park S E and Lee W K 2011 *Opt. Eng.* **50** 023602
[8] Weichman M L, Changala P B, Ye J, Chen Z, Yan M and Picqué N 2019 *J. Mol. Spectrosc.* **355** 66
[9] Cruz F C, Maser D L, Johnson T, Ycas G, Klose A, Giorgetta F R, Coddington I and Diddams S A 2015 *Opt. Express* **23** 26814
[10] Vainio M and Halonen L 2016 *Phys. Chem. Chem. Phys.* **18** 4266
[11] Nishiyama A, Ishikawa D and Misono M 2013 *J. Opt. Soc. Am. B* **30** 2107
[12] Leopardi H, Davila-Rodriguez J, Quinlan F, Olson J, Sherman J A, Diddams S A and Fortier T M 2017 *Optica* **4** 879
[13] Lezius M, Wilken T, Deutsch C, *et al*. 2016 *Optica* **3** 1381
[14] Cundiff S T and Ye J 2003 *Rev. Mod. Phys.* **75** 325
[15] Newbury N R and Swann W C 2007 *J. Opt. Soc. Am. B* **24** 1756
[16] Baumann E, Giorgetta F R, Nicholson J W, Swann W C, Coddington I and Newbury N R 2009 *Opt. Lett.* **34** 638
[17] Xin M, Li N, Singh N, Ruocco A, Su Z, Magden E S, Notaros J, Vermeulen D, Ippen E P, Watts M R and Kärtner F X 2019 *Light Sci. Appl.* **8** 122
[18] Droste S, Ycas G, Washburn B R, Coddington I and Newbury N R 2016 *Nanophotonics* **5** 196
[19] Kim J W and Song Y 2016 *Adv. Opt. Photon.* **8** 465
[20] Kitajima S, Jung K and Nishizawa N 2024 *Sci. Rep.* **14** 7108
[21] Raabe N, Feng T, Mero M, Tian H, Song Y, Hänsel W, Holzwarth R, Sell A, Zach A and Steinmeyer G 2017 *Opt. Lett.* **42** 1068
[22] Cao X, Zhou J, Cheng Z, Li S and Feng Y 2023 *Laser & Photon. Rev.* **17** 2300537
[23] Zhou J, Pan W, Fu X, Zhang L and Feng Y 2019 *Opt. Fiber Technol.* **52** 101963
[24] Zhang Q, Hou Y, Song W, Wang X, Blair C, Chen X, Li J, Zhao C and Song W 2021 *Opt. Express* **29** 3221
[25] Zhao J, Guiraud G, Pierre C, Floissat F, Casanova A, Hreibi A, Chaibi W, Traynor N, Boullet J and Santarelli G 2018 *Appl. Phys. B* **124** 114
[26] Li M, Yang X, Rao B, Yan L, Chen X, Yuan R, Zhang P, Zhang Y and Liu T 2023 *Front. Phys* **11** 1044842
[27] Mayer A S, Grosinger W and Fellinger J 2020 *Opt. Express* **28** 18946
[28] Fang F, Li M, Lin P, Chen W, Liu N, Lin Y, Wang P, Liu K, Suo R and Li T 2015 *Metrologia* **52** 454
[29] Fang F, Liu N, Liu K, Chen W, Suo R and Li T 2016 *Int. J. Mod. Phys. Conf. Ser.* **723** 012009
[30] Deng Z, Liu Y, Zhu Z, Luo D, Gu C, Zhou L, Xie G and Li W 2021 *Opt. Laser Technol.* **138** 106906